

Feasibility of subendocardial and subepicardial myocardial perfusion measurements in healthy normals with ^{15}O -labeled water and positron emission tomography

Ilse A. Vermeltfoort, MD,^a Pieter G. Raijmakers, PhD,^a Mark Lubberink, PhD,^{a,c} Tjeerd Germans, PhD,^b Albert C. van Rossum, PhD,^b Adriaan A. Lammertsma, PhD,^a and Paul Knaapen, PhD^b

Background. Positron emission tomography (PET) enables robust and reproducible measurements of myocardial blood flow (MBF). However, the relatively limited resolution of PET till recently prohibited distinction between the subendocardial and the subepicardial layers in non-hypertrophied myocardium. Recent developments in hard- and software, however, have enabled to identify a transmural gradient difference in animal experiments. The aim of this study is to determine the feasibility of subendocardial and subepicardial MBF in normal human hearts assessed with ^{15}O -labeled water PET.

Methods. Twenty-seven healthy subjects (mean age 41 ± 13 years; 11 men) were studied with ^{15}O -labeled water PET to quantify resting and hyperaemic (adenosine) MBF at a subendocardial and subepicardial level. In addition, cardiac magnetic resonance imaging was performed to determine left ventricular (LV) volumes and function.

Results. Mean rest MBF was 1.46 ± 0.49 in the subendocardium, and 1.14 ± 0.342 mL \cdot min⁻¹ \cdot g⁻¹ in the subepicardium ($P < .001$). MBF during vasodilation was augmented to a greater extent at the subepicardial level (subendocardium vs subepicardium: 3.88 ± 0.86 vs 4.14 ± 0.88 mL \cdot min⁻¹ \cdot g⁻¹, $P = .013$). The endocardial-to-epicardial MBF ratio decreased significantly during hyperaemia (1.35 ± 0.23 to 1.12 ± 0.20 , $P < .001$). Hyperaemic transmural MBF was inversely correlated with left ventricular end-diastolic volume index (LVEDVI) ($r^2 = 0.41$, $P = .0003$), with greater impact however at the subendocardial level.

Conclusions. ^{15}O -labeled water PET enables MBF measurements with distinction of the subendocardial and subepicardial layers in the normal human heart and correlates with LVEDVI. This PET technique may prove useful in evaluating patients with signs of ischaemia due to coronary artery disease or microvascular dysfunction. (J Nucl Cardiol 2011;18:650–6.)

Key Words: Positron emission tomography • imaging • coronary microcirculation • myocardial blood flow • subendocardial

INTRODUCTION

The subendocardium is most susceptible to perfusion impairment and ischaemia principally occurs in the subendocardium before advancing to the subepicardial layer.¹ Subendocardial perfusion imaging may therefore be an important technique to enhance the sensitivity for detection of myocardial ischaemia. Presently, quantification of regional myocardial blood flow (MBF) is available with tracers such as ^{15}O -labeled water (H_2^{15}O) and positron emission tomography (PET). H_2^{15}O PET may therefore serve as a tool for quantifying impairments in microcirculatory vasodilator reactivity.^{2,3}

Recent advances in cardiac PET hard- and software enable to distinguish between perfusion of the

See related editorial, pp. 544–546

From the Department of Nuclear Medicine & PET Research,^a Department of Cardiology,^b VU University Medical Centre, Amsterdam, The Netherlands; and PET Centre,^c Uppsala University Hospital, Uppsala, Sweden.

Received for publication Feb 4, 2011; final revision accepted Apr 2, 2011.

Reprint requests: Ilse A. Vermeltfoort, MD, Department of Nuclear Medicine & PET Research, VU University Medical Centre, de Boelelaan 1117, 1007 MB Amsterdam, The Netherlands; *i.vermeltfoort@vumc.nl*. 1071-3581/\$34.00

Copyright © 2011 The Author(s). This article is published with open access at Springerlink.com

doi:10.1007/s12350-011-9375-y

subendocardial and subepicardial layers in animal experiments and patients with left ventricular hypertrophy.^{4,5} However, data in normal human hearts are scarce. We studied the feasibility of subendocardial and subepicardial MBF measurements in a group of healthy volunteers using H₂¹⁵O PET during both rest and vasodilator stress.

METHODS

Patient Population

Twenty-seven healthy subjects were studied. None of the patients had a history of cardiovascular disease, all were non-smokers, and none had any other cardiovascular risk factor. Accordingly, none of the volunteers was receiving any form of treatment. All underwent a physical examination, electrocardiography, laboratory analysis, and echocardiography revealing no abnormalities. The characteristics of the study group are given in Table 1. All subjects gave written informed consent, and the protocol was approved by the Medical Ethics Committee of the VU University Medical Centre.

Imaging Protocol

PET. All scans were performed in 2D mode using an ECAT EXACT HR + (Siemens/CTI, Knoxville, TN, USA). The subjects were monitored constantly with single-lead electrocardiography, and blood pressure was measured every minute. After a transmission scan, 1100 MBq of H₂¹⁵O was injected intravenously under resting conditions and subsequently during pharmacologically induced hyperaemia (adenosine, 140 µg · kg⁻¹ · min⁻¹), as described previously in detail.^{4,6} Emission data were corrected for physical decay of ¹⁵O and for dead time, scatter, randoms, and photon

attenuation. The H₂¹⁵O emission sinograms were reconstructed using filtered back-projection with a Hanning filter at 0.5 of the Nyquist frequency, resulting in a transaxial spatial resolution of ~6.5 mm full-width at half-maximum.

Cardiac magnetic resonance (CMR) imaging. Scans were performed on a 1.5-T whole body scanner (Magnetom Sonata, Siemens, Erlangen, Germany) using a six-element phased-array radio-frequency receiver body coil. All images were electrocardiographically gated and acquired during repeated breath holds in mild expiration of 10-15 s, depending on heart rate. After localization of scout scans, cine images were acquired with a segmented balanced steady-state free-precession sequence. The image parameters were as follows: 5 mm slice thickness, 5 mm slice gap, <50 ms temporal resolution, 3.2 ms repetition time, 1.54 ms echo time, 60° flip angle, and 1.3 × 1.6 mm typical image resolution. After three long-axis view cines (2-, 3-, and 4-chamber views), a stack of 10-12 LV short-axis cines were acquired for full coverage of the LV.⁷

Data Analysis

PET. Transaxial parametric MBF images were generated as described previously.⁸ These images were reoriented according to the anatomic axis of the heart, and displayed as short-axis slices. The same reslicing parameters were applied to the dynamic H₂¹⁵O images. Region of interests (ROIs) on these images were defined as septal, anterior, lateral, and inferior walls of the LV in the basal, mid, and apical planes, based on the 16-segment model of the AHA/ACC.⁹ Additional ROIs were defined for the LA and right ventricular chamber. This latter set of ROIs was projected onto the dynamic H₂¹⁵O images to generate image-derived input functions. The standard single-tissue compartment model, together with these input functions, was used to determine MBF (mL · min⁻¹ · g⁻¹ of perfusable tissue) for all myocardial tissue time-activity curves. The subendocardial and subepicardial layers were identified by dividing the myocardial ROIs by a central line (Figure 1). Coronary flow reserve (CFR) was calculated as the ratio of hyperaemic to resting MBF. A subendocardial to subepicardial MBF ratio was additionally calculated. Because resting MBF is determined by cardiac workload, global baseline MBF corrected for the rate pressure product (RPP) was also calculated (MBF/RPP) × 10⁴.¹⁰ Coronary vascular resistance (CVR) was calculated as the ratio of mean arterial pressure to MBF for both the subendocardial and the subepicardial layers of the myocardium.³

CMR imaging. Epicardial and endocardial contours were manually drawn on all end-diastolic (ED) and end-systolic (ES) LV short-axis images for LV volume analysis. Global LV function parameters, including ED Volume (LVEDV), ED volume adjusted for bsa (LVEDVI), ES volume (LVESV), ejection fraction (LVEF), and myocardial mass, were derived from epicardial and endocardial contours on the cine images using of the MASS software package (Mass 5.0, Medis, Leiden, The Netherlands).

Table 1. Characteristics of normal subjects (n = 27)

Characteristics	Mean ± SD
Age (years)	41 ± 13
Sex (M/F)	11/16
LVEF (%)	61 ± 5
LVEDV (mL)	71 ± 17
LVEDV (mL)	180 ± 34
Mean LV mass (g)	96 ± 24
Length (cm)	177 ± 9
Weight (kg)	74 ± 13
BSA (m ²)	1.9 ± 0.2

LVEDV, Left ventricular end-diastolic volume; LVEF, left ventricular ejection fraction; LVESV, left ventricular end-systolic volume; BSA, body surface area.

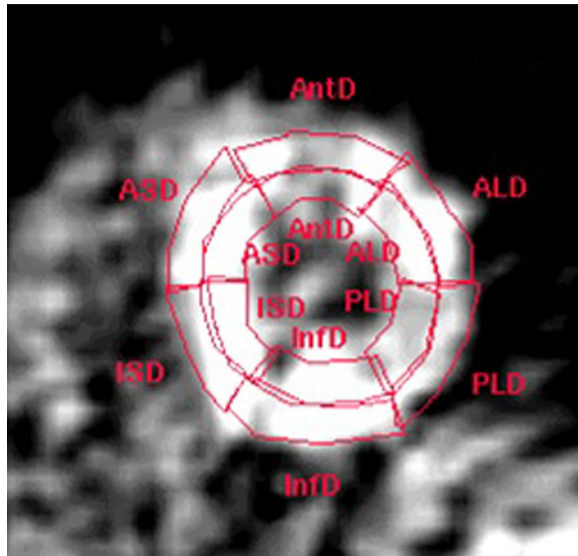


Figure 1. Example of delineation of subendocardial and subepicardial border on a parametric MBF image in short axis view at the midventricular level.

Statistics

Values are expressed as means \pm SD. For comparison of two data sets, a paired or unpaired Student's *t* test was performed where appropriate. Multiple data sets were compared using multivariate ANOVA, and specific differences were identified by a Student's *t* test corrected for multiple comparisons with the Bonferroni inequality adjustment. Linear regression was used to analyze the relationships between variables. All analyses were performed using SPSS 14 (SPSS, Chicago, IL, USA). Significant differences were defined as $P < .05$.

RESULTS

Haemodynamic Parameters

Baseline heart rate was 65 ± 11 , increasing to 98 ± 14 BPM during adenosine infusion ($P < .001$). Baseline systolic blood pressure was 122 ± 15 , and diastolic blood pressure 71 ± 10 mm Hg. During maximum vasodilatation, systolic blood pressure decreased to 117 ± 15 and diastolic blood pressure to 64 ± 7 mm Hg (both $P < .05$ vs baseline).

Transmural MBF

Global resting transmural myocardial blood flow was 1.20 ± 0.31 and increased during hyperaemia to 3.94 ± 0.78 $\text{mL} \cdot \text{min}^{-1} \cdot \text{g}^{-1}$ ($P = .001$), yielding a CFR of 3.28 ± 0.83 . Global baseline MBF corrected for rate pressure product was 1.53 ± 0.34 $\text{mL} \cdot \text{min}^{-1} \cdot \text{g}^{-1}$.

Regional transmural heterogeneity. Baseline transmural MBF for anterior, lateral, inferior, septum, and segments was 1.30 ± 0.39 , 1.29 ± 0.37 , 1.08 ± 0.32 , and 1.11 ± 0.33 $\text{mL} \cdot \text{min}^{-1} \cdot \text{g}^{-1}$, respectively ($P = .042$ by ANOVA). Hyperaemic MBF increased to 3.54 ± 0.93 , 4.18 ± 0.90 , 3.66 ± 1.04 , and 4.10 ± 0.96 $\text{mL} \cdot \text{min}^{-1} \cdot \text{g}^{-1}$ for the different regions, respectively ($P = .035$ by ANOVA). Transmural CFR for anterior, lateral, inferior, and septum segments was 2.91 ± 0.91 , 3.85 ± 1.15 , 3.39 ± 0.74 , and 3.67 ± 1.39 ($P = .011$ by ANOVA, using post hoc bonferroni significant difference between septum vs anterior $P = .010$).

Subendocardial vs Subepicardial MBF

As shown in Figure 2 and listed in Table 2, the subendocardium displayed a significantly higher mean resting flow level of 1.46 ± 0.49 compared to the mean subepicardium level of 1.14 ± 0.42 $\text{mL} \cdot \text{min}^{-1} \cdot \text{g}^{-1}$ ($P < .001$), with an endocardial-to-epicardial ratio of 1.35 ± 0.23 . During hyperaemia, there was a significant reduction in the endocardial-to-epicardial ratio to 1.12 ± 0.20 ($P < .001$), see Figure 3. Hyperemic MBF was 3.88 ± 0.86 in the subendocardium and 4.14 ± 0.88 $\text{mL} \cdot \text{min}^{-1} \cdot \text{g}^{-1}$ in the subepicardium ($P = .013$). Hyperemic MBF increased to a greater extent at the subepicardial level compared with the subendocardial level, see Table 2. Baseline coronary vascular resistance (CVR) was 67 ± 25 $\text{mm Hg} \cdot \text{mL} \cdot \text{min}^{-1}$ and 87 ± 31 $\text{mm Hg} \cdot \text{mL} \cdot \text{min}^{-1}$ for the subendocardial and subepicardial layer, respectively. During hyperaemia CVR decreases to 22 ± 7 and 21 ± 5 $\text{mm Hg} \cdot \text{mL} \cdot \text{min}^{-1}$, respectively.

Regional subendocardial vs subepicardial MBF. Regional analysis for rest MBF revealed significant differences between the subendocardial and the subepicardial layer for all segments (all $P < .05$). During hyperaemia PET was able to distinguish perfusion differences between endocardium and epicardium only in the anterior segment ($P = .020$) in the regional analysis.

There were no differences for subendocardial MBF between the four myocardial segments for resting ($P = .054$) or hyperaemic ($P = .511$) conditions, or CFR ($P = .118$). Subepicardial MBF was distributed homogeneously during rest ($P = .082$). During hyperaemia, however, significant differences were observed ($P = .004$) where MBF was lower in the anterior segment as compared with the septum ($P = .031$) and lateral wall ($P = .009$). As a consequence, CFR in the anterior wall was also lower as compared with the septum ($P = .004$) and inferior wall ($P = .047$). No regional differences in the endo-to-epicardial ratio between segments were observed during rest ($P = .097$), whereas

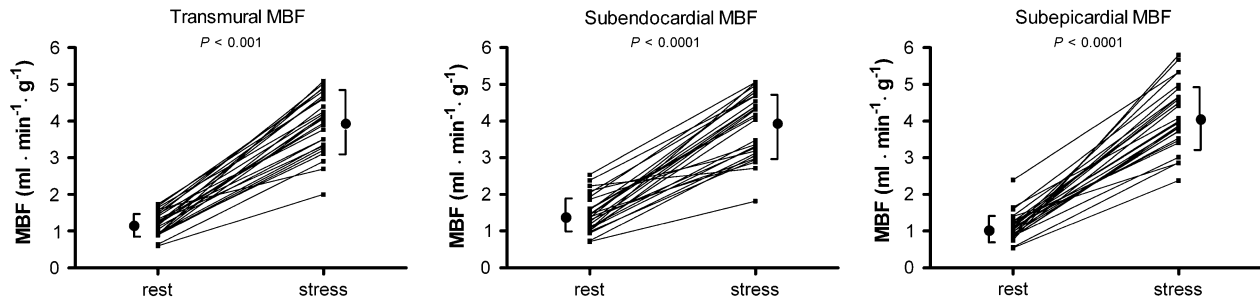


Figure 2. Transmural, subendocardial, and subepicardial myocardial blood flow (MBF) during baseline and hyperaemic conditions. *Note:* subendocardial baseline MBF is higher than subepicardial (1.46 ± 0.49 vs 1.14 ± 0.42 $\text{mL} \cdot \text{min}^{-1} \cdot \text{g}^{-1}$, $P < .001$). In contrast, hyperaemic MBF is lower in the subendocardium (3.88 ± 0.86 vs 4.14 ± 0.88 $\text{mL} \cdot \text{min}^{-1} \cdot \text{g}^{-1}$, $P < .05$).

during hyperaemia the ratio was higher in the anterior wall compared with the septum ($P = .030$).

Interrelations among PET and CMR parameters. Of the obtained PET and CMR parameters, only LVEDVI was (inversely) correlated to hyperaemic MBF (Figure 4). Of interest, the correlation was stronger at the subendocardial level as compared with the subepicardial level ($P < .05$).

DISCUSSION

The ability to distinguish subendocardial from subepicardial MBF using H_2^{15}O PET has been investigated and validated in previous studies.^{4,11,12,13} These measurements, however, have been restricted to patients with left ventricular hypertrophy to overcome the issue of partial volume effects that are caused by the relatively limited resolution of PET. Only recently, Rimoldi et al⁵ have demonstrated the feasibility to detect a transmural perfusion gradient using H_2^{15}O PET in an animal experiment with pigs characterized by comparable cardiac dimensions as normal human hearts (~ 10 mm wall thickness). This study extends to these observations and demonstrates that such a transmural perfusion gradient can similarly be detected in normal human subjects in a routine clinical setting with H_2^{15}O PET.

The results show that MBF measurements in the subendocardial layer are approximately 35% higher than in the subepicardium during resting conditions. During hyperaemia, augmentation of perfusion is greater at the subepicardial level and the transmural perfusion gradient diminishes significantly, although average subendocardial MBF remains approximately 10% higher. The combination of these observations led to an overall lower CFR in the subendocardium. These results are in line with data obtained from previous animal experiments where perfusion was measured with microspheres. Under resting conditions, subendocardial MBF is indeed consistently higher as compared with the subepicardial

layer, with endo-to-epi flow ratios varying from ~ 1.1 to 1.5 .^{5,14–17} The latter observation is compatible with the fact that, under resting conditions, myocardial perfusion is autoregulated in response to varying metabolic demand. As loading conditions and, consequently, oxidative metabolism are greater in the subendocardial layer of the myocardium, resting perfusion will be augmented relative to the subepicardial layer. During hyperaemia, however, autoregulatory mechanisms are exhausted and myocardial perfusion is predominantly governed by intravascular (i.e., vascular resistance) and extravascular (i.e., diastolic perfusion time and wall stress) forces.^{3,18} As both intravascular and extravascular forces are increased in the subendocardium as compared with the subepicardial layer, a physiological transmural perfusion gradient drop can be observed during hyperaemia relative to resting conditions, as also documented in this study. Pathophysiological conditions that are associated with elevated vascular resistance, irrespective of its origin, are characterized by a greater transmural gradient reduction and subendocardial flow frequently becomes even lower than subepicardial flow.¹⁸ It is of interest to note that in this study there was an inverse correlation between LVEDV and hyperaemic MBF. Although wall stress was not determined in these healthy subjects owing to the invasive nature of such measurements, according to Laplace's law LVEDV is one of the determinants of wall stress and may therefore represent a physiological relationship between end-diastolic wall stress and hyperaemic perfusion even within the relatively small range of end-diastolic volumes in normal subjects.¹⁹ The fact that this relation was more apparent at the subendocardial level underscores this notion as wall stress progressively declines from the endo- to the epicardial level. Moreover, the relation between hyperaemic MBF and wall stress has been documented in previous studies, and subendocardial hyperaemic perfusion can (partially) be restored by lowering end-diastolic wall stress.^{4,6,12,14,20,21}

Table 2. Subendocardial (Endo) and subepicardial (Epi) myocardial blood flow ($\text{mL} \cdot \text{min}^{-1} \cdot \text{g}^{-1}$) and coronary flow reserve (CFR)

	Rest			Hyperemia*			CFR		
	Endo	Epi	P	Endo	Epi	P	Endo	Epi	P
	Endo/Epi	Endo/Epi		Endo	Epi	Endo/Epi	Endo	Epi	
Average	1.46 ± 0.49	1.14 ± 0.42	<.001	3.88 ± 0.86	4.14 ± 0.88	.013	3.14 ± 0.83	3.97 ± 1.04	<.001
Anterior	1.68 ± 0.70	1.20 ± 0.38	<.001	3.80 ± 0.99	3.36 ± 1.06 [†]	.020	2.55 ± 0.94	3.03 ± 1.10 [‡]	.018
Lateral	1.57 ± 0.65	1.27 ± 0.54	.002	4.06 ± 0.96	4.28 ± 0.90	.173	2.89 ± 0.96	3.62 ± 0.87	<.001
Inferior	1.35 ± 0.46	0.98 ± 0.33	<.001	3.66 ± 1.06	3.65 ± 1.20	.954	3.00 ± 1.24	4.05 ± 1.72	<.001
Septum	1.30 ± 0.45	1.08 ± 0.49	.026	3.89 ± 0.98	4.16 ± 0.94	.107	3.25 ± 1.12	4.35 ± 1.57	<.001
P (ANOVA)	.054	.082	.097	.511	.004	.118	.118	.004	.004

* $P < .001$ hyperaemia vs rest for all values; [†] $P < .05$ vs septum and lateral wall; [‡] $P < .05$ vs septum and inferior wall; [¶] $P = .030$ vs septum.

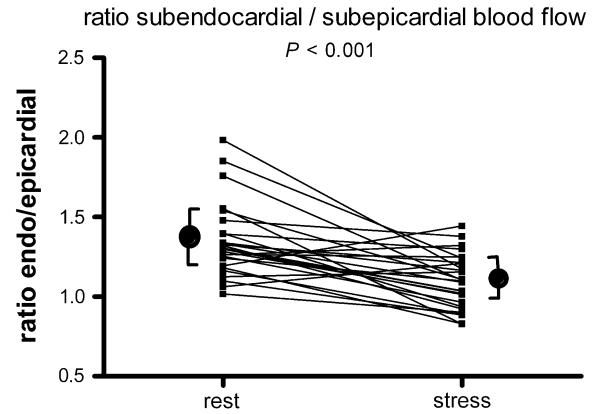


Figure 3. Endocardial-to-epicardial myocardial blood flow ratio during baseline and hyperaemic conditions. During hyperaemia, there was a significant reduction in the endocardial-to-epicardial ratio compared to rest (rest ratio 1.35 ± 0.23 vs stress ratio 1.12 ± 0.20 $P < .001$).

On average, transmural resting and hyperaemic MBF values, and hence CFR, were comparable to a previously reported large cohort of normal subjects studied with H_2^{15}O PET.²² Furthermore, some heterogeneity in both resting and hyperaemic MBF could be detected. Although these regional variations in perfusion may reflect a biological phenomenon, some technical considerations must be taken into account. The model to quantify MBF contains an intrinsic correction for spillover from blood activity from both the left and the right ventricular cavity, but not from adjacent tissue. This means that tissue surrounding the myocardium (such as the chest wall for the anterior segments, lung tissue for the lateral wall, and abdominal organs for the inferior wall) could influence perfusion values and lead to slight heterogeneity. Region definition in smaller areas of interest, such as with subendocardial and subepicardial flow measurements, will introduce more noise and potentially augment spillover artifacts from adjacent tissue. Moreover, spillover of activity between myocardial layers does also occur. Simulation models and in vivo studies have revealed that the latter will result in underestimation of the transmural gradient.^{5,11}

It is therefore expected that the observed perfusion differences between layers in this study will actually be even more pronounced. Another issue concerns the model-based corrections for partial volume.²³ This correction is warranted owing to the relatively limited resolution of PET relative to the normal myocardial wall thickness. This correction is fairly robust and reproducible for transmural flow measurement, but might pose limitations for smaller regions comprising only half of the myocardial wall.²⁴ Obviously, more studies are warranted pertaining reproducibility. Finally, but of

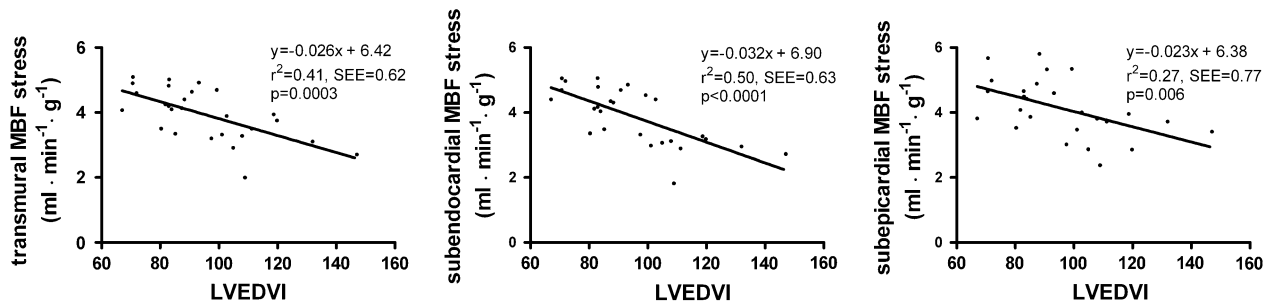


Figure 4. Hyperaemic transmural, subendocardial, and subepicardial MBF in relation to left ventricular end-diastolic volume index (LVEDVI).

paramount importance, there is the potential of cardiac and respiratory gating to further enhance the accuracy of subendocardial and subepicardial flow measurements. This study was conducted without cardiac or respiratory gating as count statistics per gated frame would become insufficient for dynamic quantitative $H_2^{15}O$ perfusion imaging. Nonetheless, recent studies have clearly demonstrated that such gating sequences substantially improve spatial resolution.^{25,26} With the aid of list mode acquisition as well as time-of-flight sequences, future studies will certainly need to focus on the applicability of cardiac and respiratory gating to increase the spatial resolution in dynamic quantitative PET imaging to facilitate measurements of transmural myocardial perfusion gradients.^{27,28}

CLINICAL IMPLICATIONS

It seems that PET measurements of subendocardial/subepicardial flow ratio can be used as an index for subendocardial perfusion, using the subepicardial perfusion as a reference. Normal values of subendocardial perfusion and the subendocardial/subepicardial flow ratio are of potential clinical importance for identifying patients at risk of subendocardial ischaemia. In a recent study, a decreased subendocardial/subepicardial flow ratio was found by PET for patients with hypertrophied hearts indicating microvascular dysfunction.⁴ Coronary microvascular dysfunction is probably also the cause of the angina in a subgroup of cardiac syndrome X patients (angina-like chest pain in the absence of obstructive CAD).^{29,30} Rosen et al³¹ reported however that no significant transmural MBF differences existed between cardiac syndrome X patients and controls using ^{15}O -labeled water PET. However, this does not exclude subendocardial ischaemia in this group of patients.^{32,33} Further studies using PET may reveal possible subendocardial ischemia in patients with cardiac syndrome X. Hence quantification of regional myocardial blood flow may be clinically useful not only for assessing the extent

and severity of coronary vascular disease, but also to detect and measure impairments in microcirculatory function in non-coronary cardiac disease. The prognostic significance of transmural microcirculatory dysfunction in the absence of CAD, however, remains to be assessed.

CONCLUSIONS

This study demonstrates the feasibility of using ^{15}O -labeled water positron emission tomography (PET) to measure myocardial blood flow in both the subendocardial and the subepicardial layers of a left ventricle of normal thickness. This PET technique may prove useful in evaluating patients with signs of ischaemia due to microvascular dysfunction.

Acknowledgment

We thank Dr R. J. H. Wanhill PhD for his critical review and editing of the manuscript.

Open Access

This article is distributed under the terms of the Creative Commons Attribution Noncommercial License which permits any noncommercial use, distribution, and reproduction in any medium, provided the original author(s) and source are credited.

References

1. Algranati D, Kassab GS, Lanir Y. Why is the subendocardium more vulnerable to ischemia? A new paradigm. *Am J Physiol Heart Circ Physiol* 2010;300:H1090-100.
2. Camici PG, Rimoldi OE. The clinical value of myocardial blood flow measurement. *J Nucl Med* 2009;50:1076-87.
3. Knaapen P, Camici PG, Marques KM, Nijveldt R, Bax JJ, Westerhof N, et al. Coronary microvascular resistance: Methods for its quantification in humans. *Basic Res Cardiol* 2009;104:485-98.

4. Knaapen P, Germans T, Camici PG, Rimoldi OE, ten Cate FJ, ten Berg JM, et al. Determinants of coronary microvascular dysfunction in symptomatic hypertrophic cardiomyopathy. *Am J Physiol Heart Circ Physiol* 2008;294:H986-93.
5. Rimoldi O, Schafers KP, Boellaard R, Turkheimer F, Stegger L, Law MP, et al. Quantification of subendocardial and subepicardial blood flow using ^{15}O -labeled water and PET: Experimental validation. *J Nucl Med* 2006;47:163-72.
6. Knaapen P, van Campen LM, de Cock CC, Gotte MJ, Visser CA, Lammertsma AA, et al. Effects of cardiac resynchronization therapy on myocardial perfusion reserve. *Circulation* 2004;110:646-51.
7. Hofman HA, Knaapen P, Boellaard R, Bondarenko O, Gotte MJ, van Dockum WG, et al. Measurement of left ventricular volumes and function with O-15 -labeled carbon monoxide gated positron emission tomography: Comparison with magnetic resonance imaging. *J Nucl Cardiol* 2005;12:639-44.
8. Boellaard R, Knaapen P, Rijbroek A, Luurtsema GJ, Lammertsma AA. Evaluation of basis function and linear least squares methods for generating parametric blood flow images using ^{15}O -water and Positron Emission Tomography. *Mol Imaging Biol* 2005;7:273-85.
9. Cerqueira MD, Weissman NJ, Dilsizian V, Jacobs AK, Kaul S, Laskey WK, et al. Standardized myocardial segmentation and nomenclature for tomographic imaging of the heart: A statement for healthcare professionals from the Cardiac Imaging Committee of the Council on Clinical Cardiology of the American Heart Association. *J Nucl Cardiol* 2002;9:240-5.
10. Knaapen P, Boellaard R, Gotte MJ, Dijkmans PA, van Campen LM, de Cock CC, et al. Perfusable tissue index as a potential marker of fibrosis in patients with idiopathic dilated cardiomyopathy. *J Nucl Med* 2004;45:1299-304.
11. Choudhury L, Elliott P, Rimoldi O, Ryan M, Lammertsma AA, Boyd H, et al. Transmural myocardial blood flow distribution in hypertrophic cardiomyopathy and effect of treatment. *Basic Res Cardiol* 1999;94:49-59.
12. Rajappan K, Rimoldi OE, Dutka DP, Ariff B, Pennell DJ, Sheridan DJ, et al. Mechanisms of coronary microcirculatory dysfunction in patients with aortic stenosis and angiographically normal coronary arteries. *Circulation* 2002;105:470-6.
13. Timmer SA, Knaapen P, Lubberink M, Lammertsma AA, Germans T, Dijkmans PA, et al. Effects of alcohol septal ablation on coronary microvascular function and myocardial energetics in hypertrophic obstructive cardiomyopathy [abstract]. AHA poster presentation, Chicago 2010.
14. Hittinger L, Mirsky I, Shen YT, Patrick TA, Bishop SP, Vatner SF. Hemodynamic mechanisms responsible for reduced subendocardial coronary reserve in dogs with severe left ventricular hypertrophy. *Circulation* 1995;92:978-86.
15. Duncker DJ, Ishibashi Y, Bache RJ. Effect of treadmill exercise on transmural distribution of blood flow in hypertrophied left ventricle. *Am J Physiol* 1998;275:H1274-82.
16. Pagny JY, Peronnet F, Beliveau L, Sestier F, Nadeau R. Systemic and regional blood flows during graded treadmill exercise in dogs. *J Physiol (Paris)* 1986;81:368-73.
17. White FC, Roth DM, Bloor CM. Coronary collateral reserve during exercise induced ischemia in swine. *Basic Res Cardiol* 1989;84:42-54.
18. Duncker DJ, Bache RJ. Regulation of coronary blood flow during exercise. *Physiol Rev* 2008;88:1009-86.
19. Gaasch WH. Left ventricular radius to wall thickness ratio. *Am J Cardiol* 1979;43:1189-94.
20. Knaapen P, Gotte MJ, Paulus WJ, Zwanenburg JJ, Dijkmans PA, Boellaard R, et al. Does myocardial fibrosis hinder contractile function and perfusion in idiopathic dilated cardiomyopathy? PET and MR imaging study. *Radiology* 2006;240:380-8.
21. Rajappan K, Rimoldi OE, Camici PG, Bellenger NG, Pennell DJ, Sheridan DJ. Functional changes in coronary microcirculation after valve replacement in patients with aortic stenosis. *Circulation* 2003;107:3170-5.
22. Chareonthaitawee P, Kaufmann PA, Rimoldi O, Camici PG. Heterogeneity of resting and hyperemic myocardial blood flow in healthy humans. *Cardiovasc Res* 2001;50:151-61.
23. Iida H, Kanno I, Takahashi A, Miura S, Murakami M, Takahashi K, et al. Measurement of absolute myocardial blood flow with H_2^{15}O and dynamic positron-emission tomography. Strategy for quantification in relation to the partial-volume effect. *Circulation* 1988;78:104-15.
24. Kaufmann PA, Gneccchi-Ruscione T, Yap JT, Rimoldi O, Camici PG. Assessment of the reproducibility of baseline and hyperemic myocardial blood flow measurements with ^{15}O -labeled water and PET. *J Nucl Med* 1999;40:1848-56.
25. Kokki T, Sipila HT, Teras M, Noponen T, Durand-Schaefer N, Klen R, et al. Dual gated PET/CT imaging of small targets of the heart: Method description and testing with a dynamic heart phantom. *J Nucl Cardiol* 2010;17:71-84.
26. Teras M, Kokki T, Durand-Schaefer N, Noponen T, Pietila M, Kiss J, et al. Dual-gated cardiac PET-clinical feasibility study. *Eur J Nucl Med Mol Imaging* 2010;37:505-16.
27. Buther F, Dawood M, Stegger L, Wubbeling F, Schafers M, Schober O, et al. List mode-driven cardiac and respiratory gating in PET. *J Nucl Med* 2009;50:674-81.
28. Mullani NA. Additional gains with time-of-flight PET at high counting rates: Lessons learned from early time-of-flight PET systems. *J Nucl Med* 2010;51:1491-3.
29. Camici PG, Crea F. Coronary microvascular dysfunction. *N Engl J Med* 2007;356:830-40.
30. Vermeltoort IA, Bondarenko O, Raijmakers PG, Odekerken DA, Kuijper AF, Zwijnenburg A, et al. Is subendocardial ischaemia present in patients with chest pain and normal coronary angiograms? A cardiovascular MR study. *Eur Heart J* 2007;28:1554-8.
31. Rosen SD, Uren NG, Kaski JC, Tousoulis D, Davies GJ, Camici PG. Coronary vasodilator reserve, pain perception, and sex in patients with syndrome X. *Circulation* 1994;90:50-60.
32. Lanza GA, Buffon A, Sestito A, Natale L, Sgueglia GA, Galiuto L, et al. Relation between stress-induced myocardial perfusion defects on cardiovascular magnetic resonance and coronary microvascular dysfunction in patients with cardiac syndrome X. *J Am Coll Cardiol* 2008;51:466-72.
33. Panting JR, Gatehouse PD, Yang GZ, Grothues F, Firmin DN, Collins P, et al. Abnormal subendocardial perfusion in cardiac syndrome X detected by cardiovascular magnetic resonance imaging. *N Engl J Med* 2002;346:1948-53.